Available online at www.sciencedirect.com
SCIENCE DIRECT®
Journal of Sound and Vibration 270 (2004) 525–538
JOURNAL OF SOUND AND VIBRATION
www.elsevier.com/locate/jsvi

Direct computation and aeroacoustic modelling of a subsonic axisymmetric jet

X. Jiang[a,*], E.J. Avital[b], K.H. Luo[b]

[a] Department of Mechanical Engineering, Brunel University, Uxbridge UB8 3PH, UK
[b] Department of Engineering, Queen Mary, University of London, Mile End Road, London E1 4NS, UK

Accepted 15 September 2003

Abstract

A numerical algorithm for acoustic noise predictions based on solving Lilley's third order wave equation in the time–space domain is developed for a subsonic axisymmetric jet. The sound field is simulated simultaneously with the source field calculation, which is based on a direct solution of the compressible Navier–Stokes equations. The computational domain includes both the nearfield and a portion of the acoustic farfield. In the simulation, the detailed sound source structure is provided by the nearfield direct numerical simulation (DNS), while the sound field is obtained from both the DNS and the numerical solution to the non-linear Lilley's equation. The source terms of Lilley's equation are used to identify the apparent sound source locations in the idealized axisymmetric low-Reynolds number jet. The sound field is mainly discussed in terms of instantaneous pressure fluctuations, frequency spectra, acoustic intensity and directivity. A good agreement is found between the predictions from the axisymmetric Lilley's equation and the DNS results for the sound field. Limitations and perspectives of the simulation are also discussed.

1. Introduction

Sound generation by aerodynamic processes, such as jets, wakes and boundary layers, is of great importance to many applications. Traditionally, aeroacoustic noise predictions relied primarily on qualitative theoretical calculations and experimental observations. Most of the theoretical calculations were carried out using the acoustic analogy introduced by Lighthill [1]. Due to the difficulties in getting detailed information on the sound source, accurate quantitative

*Corresponding author. Fax: +44-1895-256392.
E-mail address: xi.jiang@brunel.ac.uk (X. Jiang).

0022-460X/$ - see front matter
doi:10.1016/j.jsv.2003.09.045

predictions were hard to achieve. Small errors in the source terms could lead to very large errors in the acoustic prediction.

Lilley [2], among others, tried to improve the acoustic analogy by developing higher order wave equations. Lilley's equation was anticipated to improve the sound predictions by reducing the cancellation effects in the source terms and especially to improve predictions of the high-frequency sound wave scattering and refraction. Goldstein [3] reviewed the theoretical calculations based on Lilley's equation, which primarily focused on solutions in the high- and low-frequency limits. It was pointed out that certain jet noise features were well explained by solutions of Lilley's equation, such as the enhanced directionality (over predictions based on Lighthill's equation), and the zone of silence along the downstream axis for high frequencies. There were also a few recent theoretical calculations of noise generation by using the solutions to Lilley's equation, e.g., Refs. [4–6].

In recent years, computational aeroacoustics (CAA) has been developing rapidly due to the significant advancement on both computer power and numerical methods. Particularly, direct numerical simulations (DNS) provide detailed information on the source flow field, and therefore provide a possibility to yield more fundamental knowledge about the sound generation process. A direct CAA approach is to simulate the source field and sound field with the same methods. This approach was found successful for Mach wave generation by supersonic shear flows, e.g., Mitchell et al. [7] and Avital et al. [8]. This is mainly because of the relatively small differences between the source field and sound field in the energy level and dominant length scale.

Computational aeroacoustics of low subsonic jets is particularly difficult, mainly because of the very small energy of the acoustic field relative to the flow field. A useful approach for aeroacoustic predictions of subsonic jets is to compute the nearfield hydrodynamic region by solving Navier–Stokes equations, and then use an acoustic analogy to determine the farfield sound. The acoustic analogy equation and particularly its Green's function solution were identified by many as a good way to calculate the sound in this approach. However, applications of this method are limited by the numerical constraints and the cancellation effects in the source terms due to retarded-time variation [9]. Green's function method also requires linearization of the acoustic analogy equation, which takes the non-linear propagation terms as sources. This linearization, however, could result in a deterioration of the numerical accuracy.

Recently, Colonius et al. [10] used DNS to compute the acoustic field of a two-dimensional planar mixing layer and compared the results with acoustic predictions from Lilley's equation. In their work, the linearized Lilley's equation was solved in the frequency–space domain. Because the Fourier transform in time was used, only the sound that was produced after a periodic state had been reached was considered. To the best of the authors' knowledge, a numerical solution in the time–space domain of Lilley's equation has never been attempted.

The main objective of this study is to develop a numerical algorithm for jet noise predictions based on solving Lilley's equation in the time–space domain. An idealized axisymmetric low-Reynolds number jet has been investigated. The sound field is simulated simultaneously with the source field DNS, by using a time-marching technique. In this way the retarded-time variation can easily be accounted for. In order to validate the acoustic solver, the same computational domain is used for the acoustic analogy approach based on Lilley's equation and the DNS. The acoustic field is discussed in terms of the instantaneous sound field and the aeroacoustic properties such as frequency spectra, acoustic intensity and directivity.

2. Mathematical formulation

A cold jet without significant temperature variation is considered. The physical problem is similar to that of Mitchell et al. [11], in which the sound generated by vortex pairing was studied. To ease the high computational burden of computing the jet near and farfields together, only the axisymmetric case is considered. Although axisymmetric jets differ from fully three-dimensional turbulent jets, useful physical insights can be garnered from the consideration of this type of "building block" flows [11]. In the following, the governing equations used in the DNS and the third order axisymmetric Lilley's equation for the acoustic analogy are presented.

2.1. The flow equations

The flow field is described with the compressible time-dependent Navier–Stokes equations. The physical space is spanned by a cylindrical co-ordinate system (x, r, θ), where x is along the jet axis. In this work, the non-dimensional form of the governing equations is employed. Major reference quantities used in the normalization are the initial centerline velocity and jet radius. The non-dimensional quantities are: x, streamwise distance; r, radial distance; u_x, streamwise velocity; u_r, radial velocity; c, sonic speed; e, internal energy per unit mass; $E_T = \rho[e + (u_x^2 + u_r^2)/2]$, total energy; M, Mach number based on the initial centerline velocity; p, pressure; Re, Reynolds number; t, time; T, temperature; γ, ratio of specific heats, μ, dynamic viscosity; and ρ, density.

The conservation laws for mass, momentum and energy can be written in the following form:

$$\frac{\partial \mathbf{Q}}{\partial t} = -\frac{\partial \mathbf{E}}{\partial x} - \frac{1}{r}\frac{\partial (\mathbf{F}r)}{\partial r} - \mathbf{G}, \tag{1}$$

where the vectors $\mathbf{Q}$, $\mathbf{E}$, $\mathbf{F}$ and $\mathbf{G}$ are defined as

$$\mathbf{Q} = \begin{pmatrix} \rho \\ \rho u_x \\ \rho u_r \\ E_T \end{pmatrix}, \quad \mathbf{E} = \begin{bmatrix} \rho u_x \\ \rho u_x^2 + p - \tau_{xx} \\ \rho u_x u_r - \tau_{xr} \\ (E_T + p)u_x + q_x - u_x\tau_{xx} - u_r\tau_{xr} \end{bmatrix},$$

$$\mathbf{F} = \begin{bmatrix} \rho u_r \\ \rho u_x u_r - \tau_{xr} \\ \rho u_r^2 + p - \tau_{rr} \\ (E_T + p)u_r + q_r - u_r\tau_{rr} - u_x\tau_{xr} \end{bmatrix} \quad \text{and} \quad \mathbf{G} = \begin{pmatrix} 0 \\ 0 \\ (-p + \tau_{\theta\theta})/r \\ 0 \end{pmatrix}.$$

For the axisymmetric jet, it is preferable to include the centerline into the mathematical formulation. This has the advantage of applying the symmetry conditions precisely. At the centerline, a new set of equations is derived from the original equations by using l'Hôpital's rule to circumvent the singularity in the formulation [12].

The flow equations also include the perfect gas law, which is given by

$$p = \frac{\rho T}{\gamma M^2}. \tag{2}$$

2.2. The acoustic analogy equation

Lilley's equation [2] can be obtained by combining the equations describing conservation of mass and momentum for compressible flow. For the application of Lilley's equation, the usual approach was to linearize it about a time-independent parallel base flow [3–6,10]. This linearization, however, could blur the distinction between the propagation and source terms [13]. To avoid the ambiguity associated with the linearization, the non-linearized Lilley's equation is adopted in this study.

In the derivation of Lilley's equation, it is convenient to define a logarithmic pressure variable

$$\Pi = \ln \frac{p}{p_0}, \tag{3}$$

where $p_0 = 1/(\gamma M^2)$ is the ambient pressure. Assuming a constant sonic speed for the cold jet, the axisymmetric Lilley's equation in cylindrical co-ordinates can be derived as

$$\frac{\mathrm{D}}{\mathrm{D}t}\left(\frac{\mathrm{D}^2\Pi}{\mathrm{D}t^2} - c^2\nabla^2\Pi\right) + 2c^2\frac{\partial u_i}{\partial x_j}\frac{\partial}{\partial x_i}\left(\frac{\partial \Pi}{\partial x_j}\right) + 2c^2\frac{u_r}{r^2}\frac{\partial \Pi}{\partial r} = -2\gamma\frac{\partial u_i}{\partial x_j}\frac{\partial u_k}{\partial x_i}\frac{\partial u_j}{\partial x_k} - 2\gamma\frac{u_r^3}{r^3}, \tag{4}$$

where $\mathrm{D}/\mathrm{D}t = \partial/\partial t + u_i\partial/\partial x_i$ is the convective derivative. For an axisymmetric flow, $\mathrm{D}/\mathrm{D}t = \partial/\partial t + u_x\partial/\partial x + u_r\partial/\partial r$, while the other terms in Eq. (4) can be expressed as

$$\nabla^2\Pi = \frac{\partial^2\Pi}{\partial x^2} + \frac{\partial^2\Pi}{\partial r^2} + \frac{1}{r}\frac{\partial \Pi}{\partial r}, \tag{5}$$

$$\frac{\partial u_i}{\partial x_j}\frac{\partial}{\partial x_i}\left(\frac{\partial \Pi}{\partial x_j}\right) = \frac{\partial u_x}{\partial x}\frac{\partial^2\Pi}{\partial x^2} + \left(\frac{\partial u_x}{\partial r} + \frac{\partial u_r}{\partial x}\right)\frac{\partial^2\Pi}{\partial x\partial r} + \frac{\partial u_r}{\partial r}\frac{\partial^2\Pi}{\partial r^2}, \tag{6}$$

$$\frac{\partial u_i}{\partial x_j}\frac{\partial u_k}{\partial x_i}\frac{\partial u_j}{\partial x_k} = \left(\frac{\partial u_x}{\partial x}\frac{\partial u_x}{\partial x} + 2\frac{\partial u_x}{\partial r}\frac{\partial u_r}{\partial x} + \frac{\partial u_r}{\partial r}\frac{\partial u_r}{\partial r}\right)\left(\frac{\partial u_x}{\partial x} + \frac{\partial u_r}{\partial r}\right). \tag{7}$$

In Eq. (4), the left-hand side is considered to be the wave operator which contains the pressure variable Π, while the right-hand side is taken as the sound source. By applying l'Hôpital's rule, the singularity of Eq. (4) at $r = 0$ can also be circumvented.

3. Numerical implementation

The computational domain includes both the nearfield and a significant portion of the acoustic farfield. The dimensions of the computational domain are $0 \leqslant x \leqslant L_x$ and $0 \leqslant r \leqslant L_r$. In the axial direction, a sponge layer $L_{xp} < x \leqslant L_x$ is used to prevent the spurious wave reflections from the outflow boundary [12]. A grid uniformly spaced in the x direction and non-equally spaced in the r direction is used. The mapped grid in the radial direction is employed to resolve the jet nearfield flow structure and farfield sound more efficiently [14]. To avoid the risk of the numerical discretization distorting the sound field, high-order numerical methods and the appropriate boundary conditions are used for the DNS and Lilley's acoustic analogy equation.

3.1. Numerical methods for the DNS

In the DNS, the spatial differentiation of the governing equations is performed using a sixth order accurate compact (Padé) finite difference scheme with spectral-like resolution [15], which is of sixth order at inner points, fourth order at the next to boundary points and third order at the boundary. At the jet centerline $r = 0$, the formal sixth order accuracy of the numerical scheme is preserved by applying the symmetry conditions [12]. The time-dependent governing equations are integrated forward in time using a third order compact-storage fully explicit Runge–Kutta scheme [16] of the family derived by Wray [17].

The computational box is bounded by the inflow, outflow boundaries in the streamwise direction, the far side boundary in the radial direction, and the symmetry boundary at the jet centerline. Non-reflecting characteristic boundary conditions [18] are used at the inflow, outflow, and the far side radial boundaries. The symmetry conditions are applied at the jet centerline without additional characteristic boundary conditions. For the outflow boundary, it was found necessary to use a sponge layer [12] next to the boundary to control spurious wave reflections. Using a sponge layer is similar to a "sponge region" or "exit zone" at the end of the domain [7,10,11,19]. The results in the sponge layer are not truly physical and therefore are not used in the data analysis.

A hyperbolic tangent mean velocity profile is specified at the inlet $x = 0$, which is given by

$$\bar{u}_x = \tfrac{1}{2} U_0 \left\{ 1 - \tanh\left[\frac{R_0}{4\delta_2} \left(\frac{r}{R_0} - \frac{R_0}{r} \right) \right] \right\}, \tag{8}$$

where a tiny value 10^{-9} of r is used at the jet centerline instead of a zero value. Here U_0 stands for the maximum velocity at the inlet and $\delta_2 = 0.1R_0$ is chosen as the initial momentum thickness [20]. The flow field is initiated with this longitudinal velocity profile, while the initial radial velocity is taken as zero. Initially, the pressure field is assumed to be uniform.

At the inflow boundary, the flow is perturbed to induce the roll-up and pairing of vortex rings [21]. The frequencies chosen for the perturbation are the most unstable mode f_0 and its first two leading subharmonics, $f_0/2$ and $f_0/4$. For the velocity profile given by Eq. (8) with $\delta_2 = 0.1R_0$, the non-dimensional fundamental frequency used in the simulation is the same as that of Mitchell et al. [11], which is $f_0 R_0 / U_0 = 0.218$.

3.2. Numerical solution of Lilley's equation

For the numerical solution of Eq. (4), it is convenient to define

$$\Pi_1 = \Pi, \quad \Pi_2 = \frac{\mathrm{D}\Pi}{\mathrm{D}t}, \quad \Pi_3 = \frac{\mathrm{D}^2\Pi}{\mathrm{D}t^2}. \tag{9}$$

The combination of the above definitions and Eq. (4), results in

$$\frac{\partial \Pi_1}{\partial t} = \Pi_2 - u_x \frac{\partial \Pi_1}{\partial x} - u_r \frac{\partial \Pi_1}{\partial r}, \tag{10}$$

$$\frac{\partial \Pi_2}{\partial t} = \Pi_3 - u_x \frac{\partial \Pi_2}{\partial x} - u_r \frac{\partial \Pi_2}{\partial r}, \tag{11}$$

$$\frac{\partial \Pi_3}{\partial t} = -u_x \frac{\partial \Pi_3}{\partial x} - u_r \frac{\partial \Pi_3}{\partial r} + c^2 \nabla^2 \Pi_2 - c^2 \left(\frac{\partial \Pi_1}{\partial x} \nabla^2 u_x + \frac{\partial \Pi_1}{\partial r} \nabla^2 u_r \right) - 3c^2 \left[\frac{\partial u_x}{\partial x} \frac{\partial^2 \Pi_1}{\partial x^2} + \left(\frac{\partial u_x}{\partial r} + \frac{\partial u_r}{\partial x} \right) \frac{\partial^2 \Pi_1}{\partial x \partial r} + \frac{\partial u_r}{\partial r} \frac{\partial^2 \Pi_1}{\partial r^2} \right] - 3c^2 \frac{u_r}{r^2} \frac{\partial \Pi_1}{\partial r} - 2\gamma \left(\frac{\partial u_x}{\partial x} \frac{\partial u_x}{\partial x} + 2 \frac{\partial u_x}{\partial r} \frac{\partial u_r}{\partial x} + \frac{\partial u_r}{\partial r} \frac{\partial u_r}{\partial r} \right) \left(\frac{\partial u_x}{\partial x} + \frac{\partial u_r}{\partial r} \right) - 2\gamma \frac{u_r^3}{r^3}. \quad (12)$$

The spatial differentiation in Eqs. (10)–(12) is also performed by the sixth order compact finite difference scheme. Eqs. (10)–(12) are time-marched with additional artificial numerical damping terms. The time-marching is performed by the Runge–Kutta scheme as is that for the DNS. As other commonly used CAA schemes to solve the aeroacoustic equations in time [14,22], artificial numerical viscosity has to be added and an explicit term has been chosen to suppress the high wavenumber numerical instability in the time-marching of Eqs. (10) to (12). The addition of damping terms helps to stabilize the solution. That is, a solution at large step sizes may be obtained which otherwise would have been unstable. In this study, a second order damping in the form of $\varepsilon \nabla^2 \Pi_i$ has been added explicitly to the right-hand side of Eqs. (10) to (12) with $i = 1, 2, 3$, respectively, where ε is the damping coefficient. To reduce the adverse effects of damping on the solution accuracy, the damping coefficient has been kept to a minimum value by numerical tests. In the simulation, keeping the resolution high relative to the dominant sound wavelengths emitted by the jet, meant that the effect of artificial viscosity on these sound waves was negligible. This was confirmed by the good agreement achieved with the DNS which has a physical viscous term.

The initial values of Π_1, Π_2, and Π_3 are taken as zero, corresponding to the initial conditions for the flow field of the DNS. The first order wave equations are used as the boundary conditions for the axisymmetric Lilley's equation, which were found to be sufficient for the case studied.

4. Numerical results and discussion

In the simulation, the considered jet Mach number is $M = 0.4$, which is based on the initial centerline velocity. The Reynolds number based on the nozzle radius is $Re = 2500$. The ratio of specific heats used is $\gamma = 1.4$. The dimensions of the computational box used are $L_x = 85R_0$ with $L_{xp} = 70R_0$, and $L_r = 80R_0$. The grid system used is of 1701×570 nodes. The time step is limited by the Courant–Friedrichs–Lewy (CFL) condition for stability. A CFL number of 2.0 is used. In this study, grid and time-step independence tests have been performed. The results presented next are considered to be grid and time-step independent.

4.1. The nearfield flow and sound source structures

Fig. 1 shows the time traces of the jet centerline velocity for different streamwise locations. At the inflow location $x = 0$, variation of the streamwise velocity is due to the applied perturbation. It is observed that the start-up transient arrives at points downstream at progressively later times. The growth of the external perturbation is evident. The jet acts as an amplifier for the disturbance

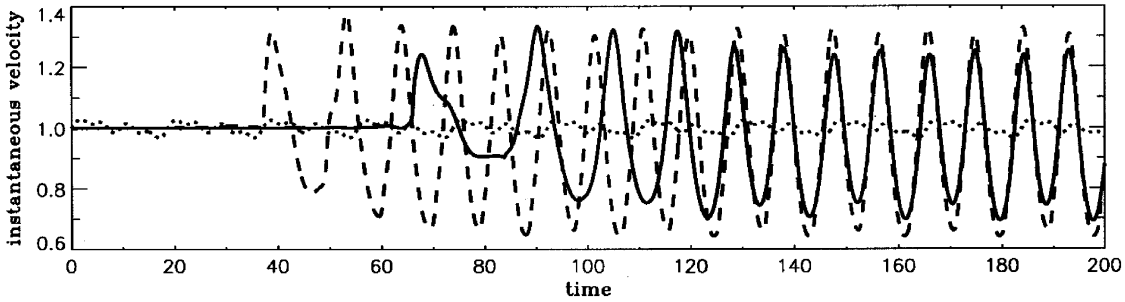

Fig. 1. Time traces of the streamwise velocity at $r = 0$ for different streamwise locations (....., $x = 0$; -----, $x = 30.0$; ——, $x = 60.0$).

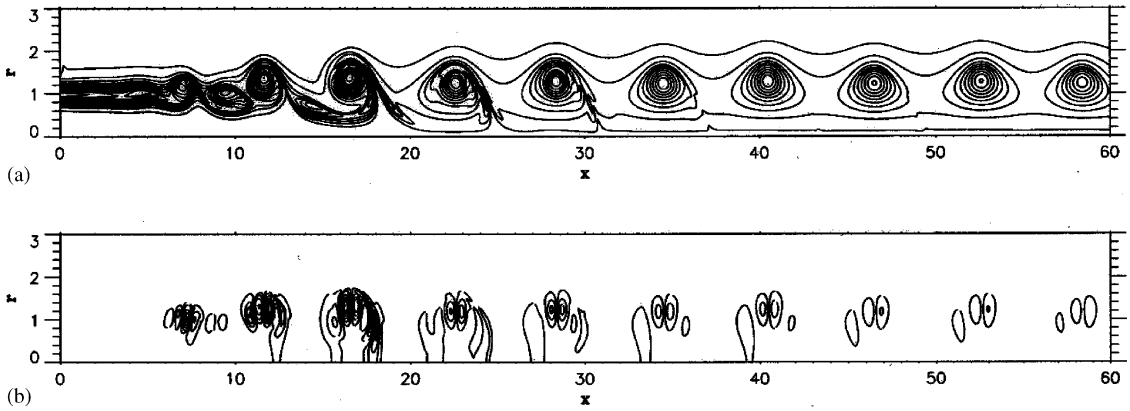

Fig. 2. The nearfield (a) vorticity structure and (b) sound source structure at $t = 200$ of the axisymmetric jet (15 contours between the minimum and maximum).

to which it is subjected. Under the effects of external disturbance with the preferred frequency, the velocity variation grows rapidly, subsequently saturates and then decays downstream. This trend is consistent with that observed experimentally by Crow and Champagne [23]. The histories of the centerline streamwise velocity shown also indicate that the jet downstream centerline velocity is dominated by the first subharmonic frequency. This is because only one vortex pairing appeared in the flow field for the flow conditions investigated [11]. The jet reaches a periodic steady state approximately after time $t = 120U_0/R_0$.

An advantage offered by DNS as a tool of CAA is that it yields the complete flow field and the exact structure of the sound source. Fig. 2 shows the nearfield vorticity and sound source structures at $t = 200$ of the axisymmetric jet after the periodic state has been reached. From Fig. 2(a), it is observed that the axisymmetric jet has a highly organized extensive vorticity field. Vortex roll up and pairing can be clearly seen. Fig. 2(b) shows the sound source structure corresponding to the vorticity shown in Fig. 2(a). The quantity shown is the summation of the right-hand side of Eq. (4). Apparently the sound source locations correspond to the flow regions with intense vorticity. This indicates that the large-scale vortical structures play an important part

in the generation of jet noise. Fig. 2 also shows that there is no apparent sound source at the jet upstream locations near the inflow boundary.

For the sake of clarity, the instantaneous profiles of the sound source at $r = 1.25$ within the jet shear layer during one period of the second subharmonic frequency are shown in Fig. 3. The instantaneous sound source terms have both positive and negative values. The intense sound source corresponds to the vortex pairing location at each individual time. Downstream, the sound source gradually becomes smaller. Due to the periodic perturbation applied at the inflow boundary, the spatially developing axisymmetric jet approaches a periodic state after the initial stage. The periodicity of the jet flow is evident in the comparison between the sound source profiles shown in Fig. 3(a) for $t = 200.0$ and Fig. 3(d) for $t = 218.3$, which are very similar in structure. From Fig. 3, it is evident that the sound source comes from the end of the jet potential core and not from the forcing applied at the inflow boundary. The sound source develops downstream of the jet potential core. This implies that it is the vortex pairing but not the inflow forcing which leads to sound generation in this axisymmetric jet.

In order to check the usual assumption of a time-independent parallel base flow made for the jet when the acoustic analogy was applied to jet noise calculations [3–6,10], Fig. 4(a) shows the time-averaged streamwise velocity contours of the axisymmetric jet from the DNS. The time interval used for the averaging is between $t_1 = 140.0$ to $t_2 = 213.4$. It is obvious that the mean flow can be roughly considered to be parallel only after the streamwise location of $x = 15.0$ where the vortex pairing occurs. Before this location, the mean flow spreads significantly in the radial direction due to the initial growth of the shear layer that invalidates the parallel mean flow assumption. This, however, does not cause any problems in the acoustic modelling performed here since the non-linearized Lilley's equation is adopted in this study through which the jet spreading effects can be taken into account.

Laufer and Yen [24] investigated the noise generation by a low-Mach-number round jet. They suggested that the acoustic sources were located within a confined volume and they were associated with the non-linear saturation of the unstable wave amplitudes of the shear layer occurring at the vortex pairing locations. To examine the statistics of the sound source distribution, contours of the root-mean-square (r.m.s.) of the sound source fluctuation are shown

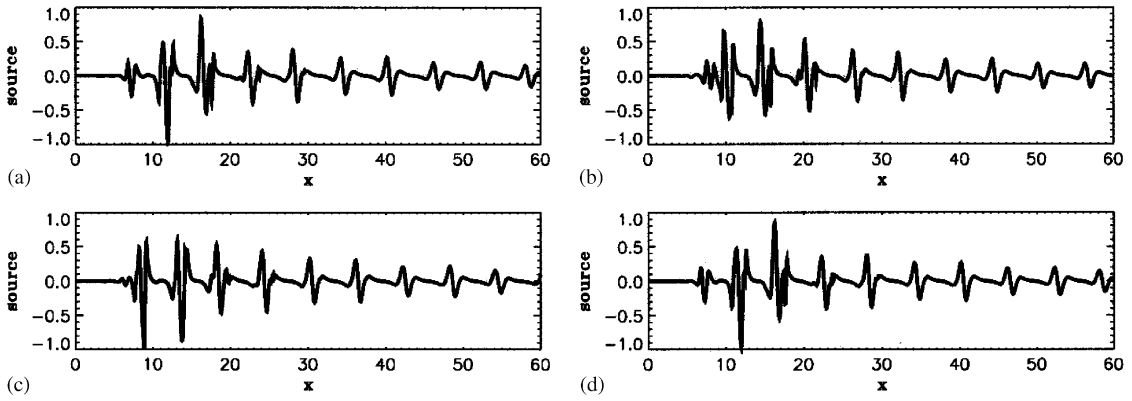

Fig. 3. Profiles of the instantaneous sound source at $r = 1.25$ during one period of the second subharmonic frequency: (a) $t = 200.0$, (b) $t = 206.1$, (c) $t = 212.2$, and (d) $t = 218.3$.

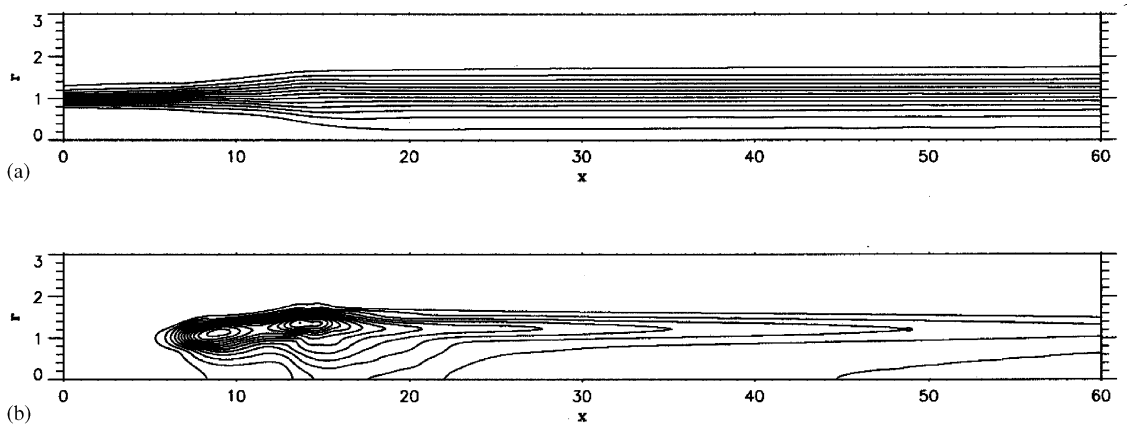

Fig. 4. (a) Time-averaged streamwise velocity and (b) the r.m.s. of the sound source fluctuation (15 contours between the minimum and maximum).

in Fig. 4(b). The r.m.s. of the fluctuation of a quantity φ is calculated as $(\overline{\varphi'^2})^{1/2} = (\overline{\varphi^2} - \bar{\varphi}^2)^{1/2}$. Here, the quantity examined is the right-hand side of Eq. (4). It can be seen that the intense sound source is located near the end of the jet potential core. The acoustic source has a large spatial distribution in the streamwise flow direction. The long length of the source and its stationary position relative to the jet potential core agree qualitatively well with the experimental observation [24].

4.2. Sound predictions from the DNS and Lilley's equation

The sound field of the axisymmetric jet is predicted by both the DNS and the solution of Lilley's equation. Figs. 5 and 6 show the farfield sound predictions from the DNS and the solution of Lilley's equation, respectively. In these figures, the pressure fluctuation contours during one period of the second subharmonic frequency are shown. It can be observed that the propagating acoustic field produced by the vortex pairing is highly directive, sound being primarily beamed downstream with a strong dependence on the angle from the jet axis. The formation of the sound beams is mainly because of the discrete sound source structure. The sound field predictions from Lilley's equation show a similar pattern to those from the DNS. The sound waves are mainly beamed downstream along the jet axis. This can be attributed to the long axial length of the source, leading to a highly directive or superdirective sound field [25]. The sound wavelength is about $8R_0$ from Figs. 5 and 6, while the source length is a factor of three to four times greater than the wavelength. This should lead to a superdirective sound field by the calculation of Avital and Sandham [26] for this Mach number.

A comparison of the time traces and frequency spectra of the pressure fluctuations at $(x = 60, r = 60)$ between the DNS and the solution of Lilley's equation is shown in Fig. 7. It is evident that only the inflow forcing frequencies are present. There is no obvious spectrum broadening and observable Doppler shift in frequency. This could be due to the axisymmetric nature of the simulation and the stationary position of the source. In an axisymmetric simulation, higher frequency turbulence could not develop which would have been developed in a fully

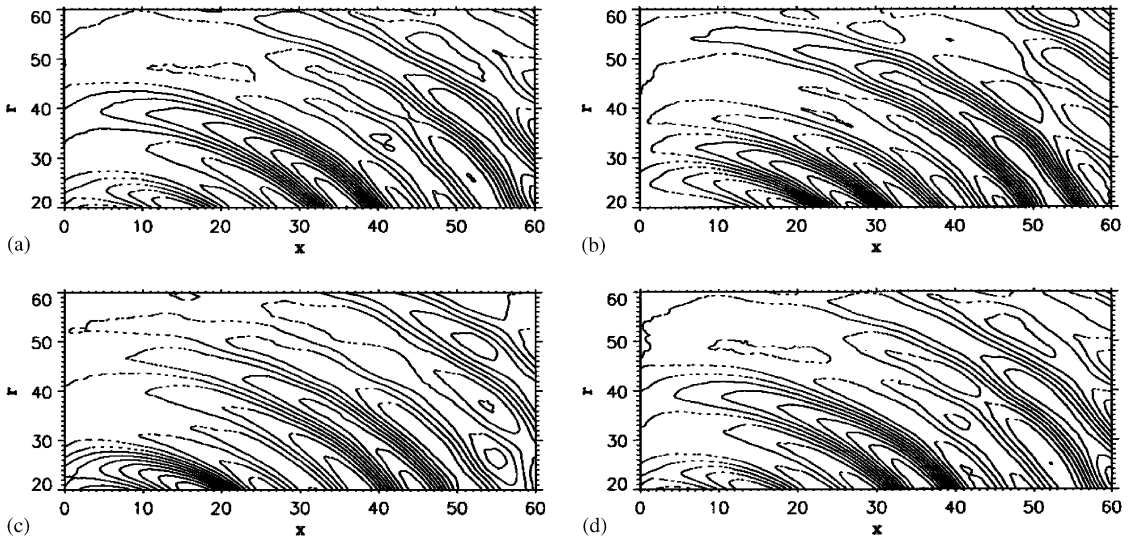

Fig. 5. The farfield sound prediction from the DNS: pressure fluctuations during one period of the second subharmonic frequency (15 contours between the minimum and maximum): (a) $t = 200.0$, (b) $t = 206.1$, (c) $t = 212.2$, and (d) $t = 218.3$.

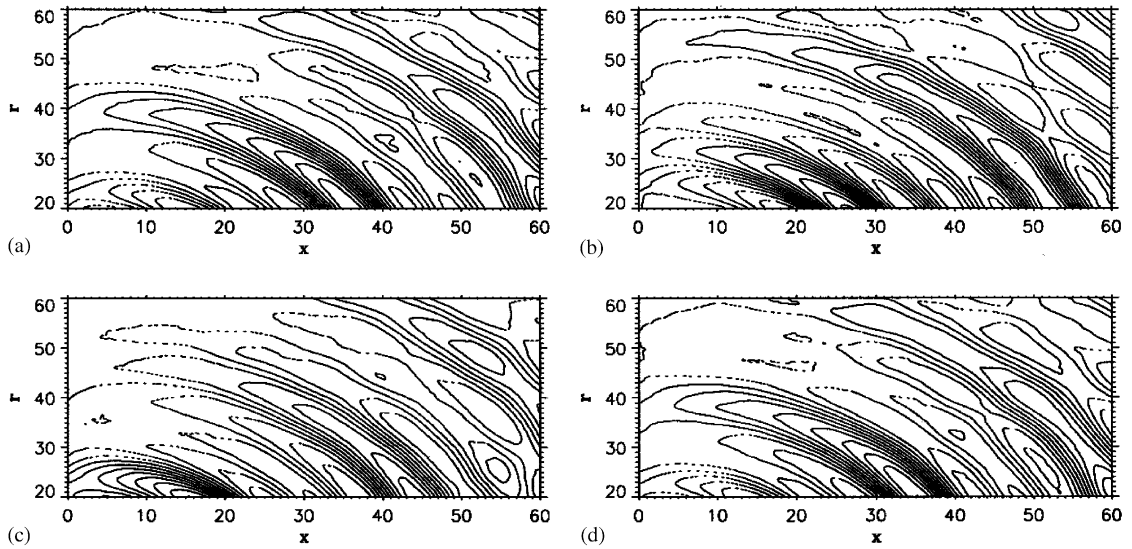

Fig. 6. The farfield sound prediction from Lilley's equation: pressure fluctuations during one period of the second subharmonic frequency (15 contours between the minimum and maximum): (a) $t = 200.0$, (b) $t = 206.1$, (c) $t = 212.2$, and (d) $t = 218.3$.

three-dimensional turbulent jet. It is also noticed that the frequency spectra obtained from the DNS and the solution of Lilley's equation are in good agreement.

There are several expressions describing the energy in acoustic fields. One of these is the mean acoustic intensity, which is the mean rate of flow of energy per unit area due to the acoustic

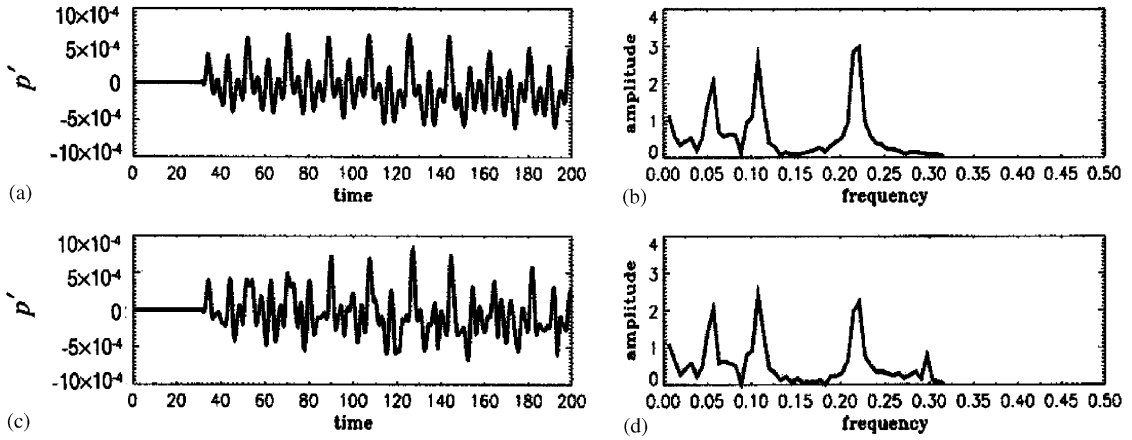

Fig. 7. Comparison of the time traces and frequency spectra of the pressure fluctuations at ($x = 60, r = 60$) between the DNS and the solution of Lilley's equation: (a) p' history from DNS, (b) Fourier spectrum from DNS, (c) p' history from Lilley's equation, and (d) Fourier spectrum from Lilley's equation.

disturbances. It can be defined in terms of the mean square pressure fluctuation [27] as

$$\bar{I} \approx \frac{1}{(t_2 - t_1)} \int_{t_1}^{t_2} \frac{\overline{p'^2}}{\rho_0 c} \, \mathrm{d}t, \tag{13}$$

where ρ_0 is the ambient density and c is the sonic speed. Based on the mean acoustic intensity, the total mean acoustic power output (the surface integral of the mean intensity) at a radial location r for an axisymmetric jet can be expressed as

$$\bar{P} = 2\pi r \int_{-\infty}^{\infty} \bar{I} \, \mathrm{d}x. \tag{14}$$

For the description of the acoustic field, the directivity of the farfield sound pressure is a useful quantity. It is a measure of the directional characteristic of a sound source. For the sound field of the axisymmetric jet, the total mean acoustic power output can also be expressed in terms of the acoustic directivity as

$$\bar{P} = \int_0^{\pi} D(\Theta) \sin \Theta \, \mathrm{d}\Theta, \tag{15}$$

where $D(\Theta)$ is the directivity, Θ is the spherical angle and $\Theta = 0$ points to the positive axial direction (jet downstream) while $\Theta = \pi$ points to the negative axial direction (jet upstream). In the above definition, it is assumed that the sound source is on the symmetry axis. Based on Eqs. (14) and (15), the directivity of the sound field at a radial location r for the axisymmetric jet can be given by

$$D(\Theta) = \frac{\bar{I} r^2}{\sin^3 \Theta}. \tag{16}$$

Fig. 8 shows the comparison of the sound field directivity distributions between the DNS and the solution of Lilley's equation at three different radial locations. The directivity in this figure is expressed in a logarithmic scale given by $10 \log_{10} D(\Theta)$. The apparent sound source location is

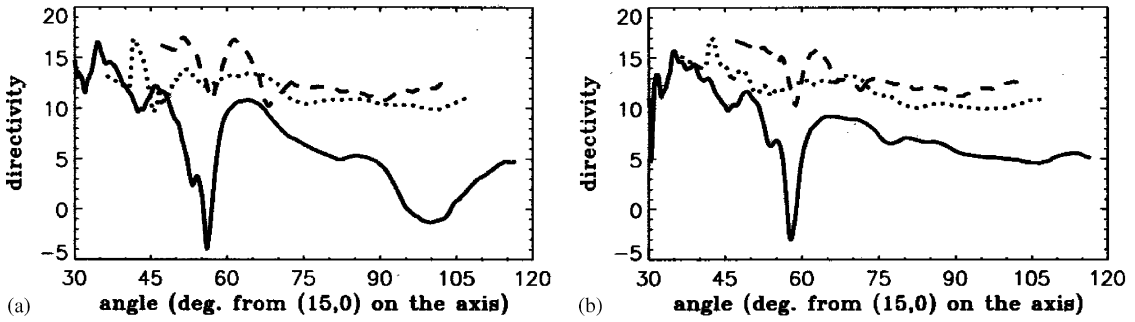

Fig. 8. Comparison of the sound field directivity distributions between (a) the DNS and (b) the solution of Lilley's equation (——, $r = 30$; ....., $r = 50$; - - - - -, $r = 70$).

taken as $x = 15R_0$ on the jet axis. It is observed that the sound radiation at lower angles (closer to the jet axis) is generally stronger than that at higher angles (away from the axis). The sound is mainly concentrated at shallow angles to the jet's downstream axis, as that observed from the contour plots shown in Figs. 5 and 6. At the radial location of $r = 30$, the lowest sound radiation occurs at an angle of $\Theta = 55°$–$60°$. This dip disappears at $r = 50$ and reappears at $r = 70$, indicating a complex sound field. The predictions from the DNS and Lilley's equation are in a fair agreement. It should be noted that aerodynamic noise computation of low-Mach number flows is susceptible to numerical errors [28] and thus such agreement is expected.

5. Conclusions and perspectives

A subsonic axisymmetric jet of Mach number 0.4 has been simulated. The sound generated by vortex pairing in this idealized axisymmetric low-Reynolds number jet is investigated by DNS and the acoustic analogy based on Lilley's equation. The insights obtained from the current axisymmetric flow configuration can aid the understanding and prediction of jet noise under more complex practical conditions. The nearfield DNS results show that the sound source locations correspond to the flow regions with intense vorticity. The strongest sound source is located in the region where the vortex pairing takes place. It is also shown that the acoustic source has a long downstream distribution. Both the DNS and numerical solution of Lilley's equation are used to predict the sound field. The results show that the acoustic field produced by the vortex pairing is highly directive. This superdirectivity of the sound field has been associated with the long length of the source and is in good agreement with previous analytical, experimental and numerical studies.

For the farfield sound prediction, the axisymmetric Lilley's equation is solved in the time-space domain for the first time. The non-linearized Lilley's equation is employed to avoid the ambiguity associated with the linearization. In this way the distinction between the propagation and source terms is made clear. Numerical solution method for the third order Lilley's equation is developed together with appropriate boundary conditions. A detailed comparison between sound predictions from Lilley's equation and DNS has been made. The good agreement between the

sound predictions from the DNS and Lilley's equation indicates the efficacy of the solution method.

The acoustic analogy based on Lilley's equation together with the solution method can be a useful tool in jet noise predictions. To reduce the high computational costs, a useful CAA approach for subsonic jets is to compute the nearfield hydrodynamic region with the DNS in a relatively small computational box in the radial direction, and use an acoustic analogy to determine the farfield sound in a relatively large domain that includes the acoustic farfield. This approach provides a possibility to perform parametric studies to elucidate the sound generation and propagation mechanisms in subsonic jets and should be considered in the future investigations. Moreover, fully three-dimensional turbulent jets should be considered based on the methodology developed from the current axisymmetric flow configuration.

Acknowledgements

This work was funded by the UK Engineering and Physical Sciences Research Council under Grant No. GR/N36097/01.

References

[1] M.J. Lighthill, On sound generated aerodynamically: I. general theory, *Proceedings of the Royal Society A* 211 (1952) 564–587.
[2] G.M. Lilley, The generation and radiation of supersonic jet noise, Report AFAPL TR-72-53, Vol. 4, US Air Force Aero Propulsion Laboratory, 1972.
[3] M.E. Goldstein, Aeroacoustics of turbulent shear flows, *Annual Review of Fluid Mechanics* 16 (1984) 263–285.
[4] A. Khavaran, Role of anisotropy in turbulent mixing noise, *American Institute of Aeronautics and Astronautics Journal* 37 (1999) 832–841.
[5] M.E. Goldstein, S.J. Leib, Emission of sound from turbulence convected by a parallel mean flow in the presence of a confining duct, *Journal of Sound and Vibration* 235 (2000) 25–42; doi: 10.1006/jsvi.1999.2912.
[6] S.J. Leib, M.E. Goldstein, Sound from turbulence convected by a parallel flow within a rectangular duct, *American Institute of Aeronautics and Astronautics Journal* 39 (2001) 1875–1883.
[7] B.E. Mitchell, S.K. Lele, P. Moin, Direct computation of Mach wave radiation in an axisymmetric supersonic jet, *American Institute of Aeronautics and Astronautics Journal* 35 (1997) 1574–1580.
[8] E.J. Avital, N.D. Sandham, K.H. Luo, Mach wave radiation by mixing layers. Part I: analysis of the sound field, *Theoretical and Computational Fluid Dynamics* 12 (1998) 73–90.
[9] E.J. Avital, N.D. Sandham, K.H. Luo, R.E. Musafir, Calculation of basic sound radiation of axisymmetric jets by direct numerical simulations, *American Institute of Aeronautics and Astronautics Journal* 37 (1999) 161–168.
[10] T. Colonius, S.K. Lele, P. Moin, Sound generation in a mixing layer, *Journal of Fluid Mechanics* 330 (1997) 375–409.
[11] B.E. Mitchell, S.K. Lele, P. Moin, Direct computation of the sound generated by vortex pairing in an axisymmetric jet, *Journal of Fluid Mechanics* 383 (1999) 113–142.
[12] X. Jiang, K.H. Luo, Direct numerical simulation of the puffing phenomenon of an axisymmetric thermal plume, *Theoretical and Computational Fluid Dynamics* 14 (2000) 55–74.
[13] J.B. Freund, Noise sources in a low-Reynolds-number turbulent jet at Mach 0.9, *Journal of Fluid Mechanics* 438 (2001) 277–305.
[14] E.J. Avital, Optimized differentiation schemes on non-uniform grids for computational aeroacoustics, *Journal of Computational Acoustics* 10 (2002) 1–15.

[15] S.K. Lele, Compact finite difference schemes with spectral-like resolution, *Journal of Computational Physics* 103 (1992) 16–42.
[16] J.H. Williamson, Low-storage Runge–Kutta schemes, *Journal of Computational Physics* 35 (1980) 48–56.
[17] A.A. Wray, Very low storage time-advancement schemes, Internal Report, NASA Ames Research Center, Moffett Field, CA, 1986.
[18] K.W. Thompson, Time dependent boundary conditions for hyperbolic systems, *Journal of Computational Physics* 68 (1987) 1–24.
[19] T. Colonius, S.K. Lele, P. Moin, Boundary conditions for direct computation of aerodynamic sound generation, *American Institute of Aeronautics and Astronautics Journal* 31 (1993) 1574–1582.
[20] A. Michalke, Survey on jet instability theory, *Progress in Aerospace Sciences* 21 (1984) 159–199.
[21] N.D. Sandham, The effect of compressibility on vortex pairing, *Physics of Fluids* 6 (1994) 1063–1072.
[22] C.K.W. Tam, Computational aeroacoustics: issues and methods, *American Institute of Aeronautics and Astronautics Journal* 33 (1995) 1788–1796.
[23] S.C. Crow, F.H. Champagne, Orderly structure in jet turbulence, *Journal of Fluid Mechanics* 48 (1971) 547–591.
[24] J. Laufer, T.C. Yen, Noise generation by a low-Mach-number jet, *Journal of Fluid Mechanics* 134 (1983) 1–31.
[25] D.G. Crighton, P. Huerre, Shear-layer pressure fluctuations and superdirective acoustic sources, *Journal of Fluid Mechanics* 220 (1990) 355–368.
[26] E.J. Avital, N.D. Sandham, A note on the structure of the acoustic field emitted by a wave packet, *Journal of Sound and Vibration* 204 (1997) 533–539.
[27] P.E. Doak, An introduction to sound radiation and its sources, in: E.J. Richards, D.J. Mead (Eds.), *Noise and Acoustic Fatigue in Aeronautics*, Wiley, London, 1968, pp. 1–42.
[28] D.G. Crighton, Computational aeroacoustics for low-Mach number flows, in: J.C. Hardin, M.Y. Hussaini (Eds.), *Computational Aeroacoustics*, Springer, New York, 1993, pp. 51–68.